The Effects of Water Vapor on the CH_3O_2 Self-Reaction and Reaction with HO_2†

Alecia M. English and Jaron C. Hansen*

Department of Chemistry and Biochemistry, Brigham Young University, Provo, Utah 84602

Joseph J. Szente and M. Matti Maricq

Chemical Engineering Department, Ford Motor Company, P.O. Box 2053, Drop 3179, Dearborn, Michigan 48121

Received: January 24, 2008; Revised Manuscript Received: July 21, 2008

The gas phase reactions of $CH_3O_2 + CH_3O_2$, $HO_2 + HO_2$, and $CH_3O_2 + HO_2$ in the presence of water vapor have been studied at temperatures between 263 and 303 K using laser flash photolysis coupled with UV time-resolved absorption detection at 220 and 260 nm. Water vapor concentrations were quantified using tunable diode laser spectroscopy operating in the mid-IR. The HO_2 self-reaction rate constant is significantly enhanced by water vapor, consistent with what others have reported, whereas the CH_3O_2 self-reaction and the cross-reaction ($CH_3O_2 + HO_2$) rate constants are nearly unaffected. The enhancement in the HO_2 self-reaction rate coefficient occurs because of the formation of a strongly bound (6.9 kcal mol^{-1}) $HO_2 \cdot H_2O$ complex during the reaction mechanism where the H_2O acts as an energy chaperone. The nominal impact of water vapor on the CH_3O_2 self-reaction rate coefficient is consistent with recent high level *ab initio* calculations that predict a weakly bound $CH_3O_2 \cdot H_2O$ complex (2.3 kcal mol^{-1}). The smaller binding energy of the $CH_3O_2 \cdot H_2O$ complex does not favor its formation and consequent participation in the methyl peroxy self-reaction mechanism.

I. Introduction

Peroxy radicals (RO_2, HO_2) play an important role as intermediates in the atmospheric oxidation and combustion of hydrocarbons. In high NO_x environments, alkylperoxy (RO_2) and hydroperoxy (HO_2) radicals react mostly with nitric oxide (NO).[1] This promotes tropospheric ozone (O_3) production, which has for many decades underlain the concern for potential respiratory health effects in urban areas.

Hydrocarbons entering the atmosphere undergo a hydrogen-atom abstraction, primarily by OH in the troposphere. The resulting alkyl radical (R) reacts almost exclusively with O_2 due to the rapid reaction rates and the abundance of O_2. The formation mechanism can be generalized by the following:

$$RH + (OH \text{ or } Cl) \rightarrow R + (H_2O \text{ or } HCl) \quad (1)$$

$$R + O_2 + M \rightarrow RO_2 + M \quad (2)$$

where M is any third body. In remote, clean areas of the troposphere, peroxy radicals terminate by reacting with HO_2.[1]

$$RO_2 + HO_2 \rightarrow ROOH + O_2 \quad (3)$$

In urban areas, reaction 3 competes with reaction 4 and its subsequent chain reaction shown below:

$$RO_2 + NO \rightarrow RO + NO_2 \quad (4)$$

$$RO + O_2 \rightarrow R_{-H}O + HO_2 \quad (5)$$

$$HO_2 + NO \rightarrow HO + NO_2 \quad (6)$$

$$NO_2 + h\nu \rightarrow O + NO \quad (7)$$

$$O + O_2 + M \rightarrow O_3 + M \quad (8)$$

Based on the mechanism described by reactions 4−8 a single RO_2 can be responsible for the production of two NO_2 molecules, which in turn can photolyze to produce two O_3 molecules when reaction 4 is dominant over reaction 3.

A. Hydroperoxy Radical. HO_2 is the simplest peroxy radical and the one found in the largest concentrations in the atmosphere (peak concentrations between 10^8 and 10^9 molecules cm^{-3}).[1] It is an important atmospheric constituent due to its role in ozone destruction and formation as well as its ability to act as a radical terminator. The presence of water vapor has been found to introduce a significant enhancement in the self-reaction rate.[2−5] The mechanism for this enhancement includes formation of an $HO_2 \cdot H_2O$ complex, which acts as an energy chaperone that removes excess energy from the activated complex on the potential energy surface and stabilizes product formation.

$$HO_2 + HO_2 \rightarrow HOOH + O_2 \quad (9)$$

$$HO_2 + HO_2 \cdot H_2O \rightarrow HOOH + O_2 + H_2O \quad (9')$$

While mechanistically water enhancement is hypothesized to occur via chaperoning, as indicated by reaction 9′, the water dependence is incorporated into the rate expression as a multiplicative factor via

$$\frac{d[HO_2]}{dt} = -2k_{9,dry}(1 + k_{9,w}[H_2O])[HO_2]^2 \quad (10)$$

where $k_{9,dry}$ is the HO_2 self-reaction rate coefficient in the absence of water vapor and $k_{9,w}$ is part of the multiplicative factor that describes the water vapor dependence on the self-reaction rate coefficient. Modeling applications that involve this reaction rate include chemical cloud models, studies of marine environments, and three-dimensional global simulations. Satellites and airborne balloons can be used to track HOOH, whose

† Part of the Stephen R. Leone Festschrift.

* Author for correspondence. E-mail: jhansen@chem.byu.edu. Fax: (801) 422-0153. Tel: (801) 422-4066.

10.1021/jp800727a CCC: $40.75
Published on Web 08/16/2008

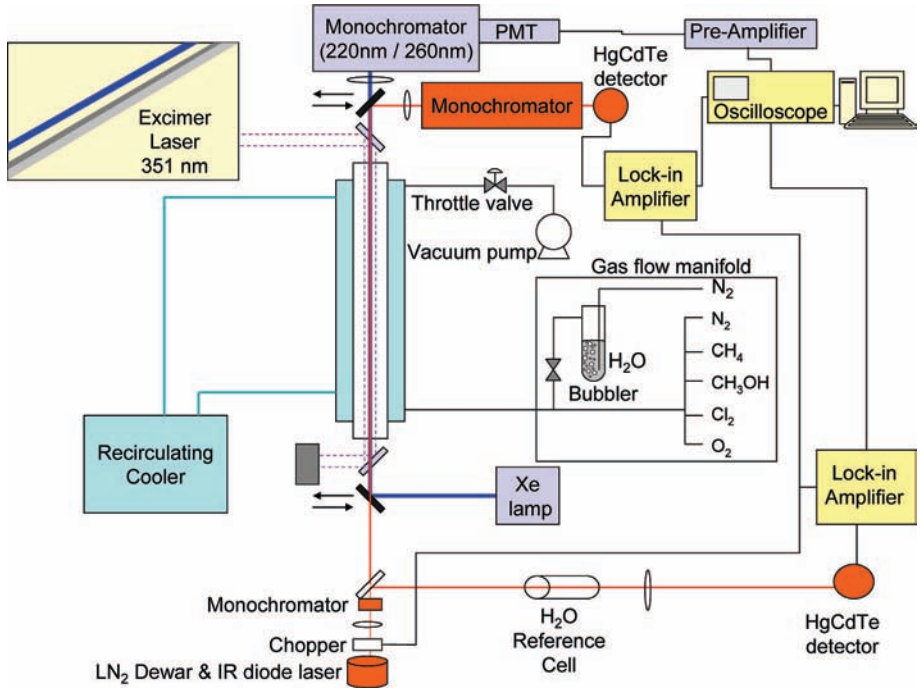

Figure 1. Schematic of UV and IR systems.

main source is the HO_2 self-reaction (reactions 9 and 9′). The photolysis of HOOH represents an additional source of HO_x radicals that help deplete ozone levels in the stratosphere. With a known [HOOH] and photolysis rate, the concentration of HO_2 can be determined from modeling, but faithful predictions require the effects of water vapor on the HO_2 self-reaction to be included. According to Stockwell,[6] if this is not accounted for, atmospheric modeling predictions underestimate hydrogen peroxide (HOOH) formation and overestimate HO_2, O_3, and other organic peroxide concentrations. His work reveals that the water vapor dependence on the overall rate coefficient accounts for up to a 75% contribution when modeling HOOH formation rates under atmospheric conditions typical of the lower troposphere and, thus, cannot be ignored.

Recently, the existence of the $HO_2 \cdot H_2O$ complex has been confirmed by Suma et al.,[7] who measured the microwave spectrum of the complex in a supersonic jet by means of a Fourier transform microwave spectrometer. The binding energy of the complex (6.9 kcal mol^{-1}) was predicted by Aloisio and Francisco[8] using *ab initio* molecular methods. Kanno et al.,[9] using frequency modulated diode laser spectroscopy, have successfully measured the equilibrium constant of the $HO_2 \cdot H_2O$ complex at 298 K. These measurements, combined with measured water vapor concentration, suggest that 20−30% of the HO_2 radicals may exist as the complex under typical atmospheric conditions.

B. Methylperoxy Radical. Because water is ubiquitous in the atmosphere with concentrations on the order of 10^{17} molecules cm^{-3}, we hypothesize that water could complex with other RO_2 radicals in much the same way it complexes with HO_2 radical.[10] The efforts of the present study are focused on the role of organic $RO_2 \cdot H_2O$ complexes, in particular the case of CH_3O_2. Methyl peroxy is formed during the photooxidation of methane (CH_4) via reactions 1 and 2. Methane is a naturally occurring component of the troposphere (~4.18×10^{13} molecules cm^{-3}).[1] The main sources are anaerobic bacterial fermentation in wetlands and enteric fermentation, mostly from cattle. Human activity may be indirectly responsible for the increase in tropospheric CH_4 over the past three decades (increasing 1−2% annually).[1]

The self-reaction of CH_3O_2 is currently considered too slow to be a significant loss process under atmospheric conditions, except in pristine environments where there are minimal NO concentrations.

$$CH_3O_2 + CH_3O_2 \rightarrow 2CH_3O + O_2 \quad (11a)$$

$$\rightarrow CH_3OH + CH_2O + O_2 \quad (11b)$$

$$k_{11} = 1 \times 10^{-13} \exp(365/T)\ cm^3\ molecule^{-1}\ s^{-1}\ \text{[ref 11]}$$

$$CH_3O_2 + CH_3O_2 \cdot H_2O \rightarrow \text{products} \quad (11')$$

If a rate enhancement existed in the presence of water vapor, then the new rate constant could have a significant effect on modeling behavior.

In a recent high level *ab initio* study, Clark et al.[10] reported on the optimized geometries, binding energies, and equilibrium constants for a series of organic peroxy radical-water complexes. Their work showed that for species with strong binding energies (~5−7 kcal mol^{-1}) a significant fraction (10−25%) of the RO_2 radicals can exist as an $RO_2 \cdot H_2O$ complex. They reported that the binding energy of the complexes is largest when the R-group in the peroxy radical includes a carbonyl (C═O) or alcohol (−OH) moiety. As a consequence of the weak binding energy between the methyl peroxy radical and water (2.3 kcal mol^{-1}), the equilibrium constant for formation of a $CH_3O_2 \cdot H_2O$ complex is very small (1.54×10^{-21} cm^3 $molecule^{-1}$, at 298 K). As a result, a methyl peroxy−water complex is not expected to form and consequently will not participate during the reaction mechanism of the CH_3O_2 self-reaction. Possible enhancement in the $CH_3O_2 + HO_2$ reaction rate was hypothesized as occurring via the formation of an $HO_2 \cdot H_2O$ complex, that is,

$$CH_3O_2 + HO_2 \rightarrow CH_3OOH + O_2 \quad (12)$$

$$k_{12} = 3.8 \times 10^{-13}\, e^{(800/T)}\ cm^3\ molecule^{-1}\ s^{-1}\ \text{[ref 12]}$$

$$CH_3O_2 + HO_2 \cdot H_2O \rightarrow CH_3OOH + O_2 + H_2O \quad (12')$$

Any rate enhancement would increase the competition between

methyl peroxy removal by HO_2 versus NO.

II. Methods

To investigate the dependence on water vapor of RO_2 radical reactions, the kinetics of the self-reactions of HO_2 and CH_3O_2, and the cross-reaction of $HO_2 + CH_3O_2$ were measured over 263−303 K at ∼200 Torr. Flash photolysis/UV spectroscopy is used to create/monitor the radicals, while tunable diode laser (TDL) spectroscopy is used to quantify water vapor concentration. Figure 1 presents a schematic representation of this system showing the components used for both the UV and IR spectroscopy measurements. All of the experiments are performed in a quartz cylindrical reaction cell (52.8 cm in length, 3.6 cm in diameter) which is wrapped in an insulated jacket connected to a recirculating cooler. K-type thermocouples are placed at the ends of the cell to monitor the temperature of the system. BaF_2 windows are used at both ends of the cell because they transmit both UV and IR light over the range of interest. The use of kinematically mounted mirrors in the optical path of the system makes it possible to switch between UV and IR detection methods without changing the position, and hence alignment, of the flow cell, light sources or detectors.

A. Peroxy Kinetics Measurements. HO_2 and CH_3O_2 are formed in the reaction cell using a gas mixture containing 4−6 Torr of 5% Cl_2/N_2, 0.2−1 Torr of CH_3OH (99.93% ACS HPLC grade) carried by N_2 or 75−100 Torr of CH_4, 20 Torr of O_2, and enough N_2 to reach a total pressure of 175 to 250 Torr. Tylan mass flow controllers adjust the gas flows of Cl_2, CH_4, O_2, and N_2 to achieve the appropriate partial pressures. The flow rates are verified by measuring the rate of pressure change with MKS pressure transducers (type 122A) when a selected gas flows into a fixed volume flask. Flow rates ranged between 3500 and 4500 sccm, which resulted in residence time of <2 s in the reaction cell. The excimer beam only photolyzed a small area (∼1 cm^2) of the 3.6 cm diameter cell: this combined with the small cross section of Cl_2 coupled with mixing of the reaction cell ensured that a fresh mixture of gas was probed with every laser shot. CH_3OH is introduced with a syringe pump (kd Scientific model 100) at a rate of 2.0−2.4 mL/h using N_2 as the carrier gas. The CH_3OH is injected into a heated line (∼373 K) of N_2 where it evaporates and mixes before being introduced into the reaction cell. The vapor concentration of CH_3OH is calculated from the molar concentration using the syringe delivery rate and the flow of the carrier gas in standard liters per minute along with the temperature of the cell, the density of methanol and other system factors. The methanol concentration is adjusted by changing the syringe delivery rate and/or the carrier gas flow rate. For the $CH_3O_2 + HO_2$ reaction, both methane and methanol are flowed and the ratio of $[CH_4]/[CH_3OH]$ determines the relative concentrations of CH_3O_2 and HO_2. This ratio is varied between 170 and 300.

A photolysis pulse from an excimer laser (Lamda Physik model Compex 205) initiates the radical chemistry. The laser employs a XeF mixture to produce 351 nm light at a pulse rate of 2 Hz and energy of 300 ± 20 mJ $pulse^{-1}$. The UV pulse photolyzes a small fraction (1−3%) of the Cl_2 to produce Cl radicals. The initial concentration of Cl is in the range of (3−7) × 10^{14} molecules/cm^3. This is measured by substituting ethane as a precursor to convert the reactive chlorine atoms to ethyl peroxy radicals, which are only slowly removed by their self-reaction. Modeling the $Cl + C_2H_6$ reaction shows that, for the conditions used in these experiments, reactions 1 and 2 convert ∼98% of the Cl radicals to ethyl peroxy radicals (2% are lost via competing reactions such as $Cl + C_2H_5O_2$). $[Cl]_0$ is derived from the $[C_2H_5O_2]$ absorbance, by converting this to concentration via its known UV cross section,[13] and correcting this for the ∼2% losses. This procedure is performed at least two times during each set of kinetic measurements to improve the certainty in $[Cl]_0$ and to ensure that it remains stable over the course of the measurements.

Subsequently CH_4 and/or CH_3OH are introduced into the reaction cell in lieu of C_2H_6, whereby H atom abstraction by the photolyzed Cl atoms produces the desired CH_3O_2 or HO_2 radicals, respectively. In the HO_2 case, formation occurs via

$$Cl + CH_3OH \rightarrow CH_2OH + HCl \quad (13)$$

$$CH_2OH + O_2 \rightarrow HO_2 + CH_2O \quad (14)$$

Reactant concentrations are chosen to minimize the peroxy radical formation time (typically <5 μs) and, thereby, separate this from the time scale of the peroxy chemistry of interest. Following their formation, the simplified reaction mechanisms for the peroxy radical reactions studied here are

$$HO_2 + HO_2 \rightarrow HOOH + O_2 \quad (9)$$

$$HO_2 + HO_2 \cdot H_2O \rightarrow HOOH + O_2 + H_2O \quad (9')$$

$$CH_3O_2 + CH_3O_2 \rightarrow 2CH_3O + O_2 \quad (11a)$$

$$\rightarrow CH_3OH + CH_2O + O_2 \quad (11b)$$

$$CH_3O_2 + CH_3O_2 \cdot H_2O \rightarrow \text{products} \quad (11')$$

and

$$CH_3O_2 + HO_2 \rightarrow CH_3OOH + O_2 \quad (12)$$

$$CH_3O_2 + HO_2 \cdot H_2O \rightarrow CH_3OOH + O_2 + H_2O \quad (12')$$

Table 1 lists the detailed reaction mechanism used to model this chemistry. It is important to note that the reaction between water vapor and chlorine is an insignificant (≪1%) loss process for either chlorine atoms or water vapor owing to the extremely small rate constant for this reaction ($k_{300K} = 2.03 \times 10^{-23}$ cm^3 $molecule^{-1}$ s^{-1}).[14] Also, it should be pointed out that photolysis of fluorine would have served as a more efficient initiator of the CH_3O_2 chemistry; however, F atoms react very quickly with water as well as O_2 resulting in secondary reactions and the formation of FO_2 radicals.

Figure 1 shows the main components and layout of the experimental apparatus. Time-resolved detection of HO_2 and CH_3O_2 radicals is made by directing the output from a Xe arc lamp (Oriel model 60010) through the reaction cell. The laser photolysis beam path is aligned to pass coaxially with the UV probe path by the use of dielectric mirrors which reflect the 351 nm photolysis beam while passing all other UV wavelengths (with the exclusion of a ±15 nm band centered around 351 nm). UV light absorption is detected by a monochromator (Instruments SA, Inc. model HR 320, grating 147 line/mm) and photomultiplier tube (EMI 9558QB). The signal is amplified and sent to a digital oscilloscope. The concentration of CH_3O_2 radicals is measured by monitoring the signal at 260 nm, and HO_2 is monitored at 220 nm. These wavelengths are used to distinguish between the two radicals based on their UV cross sections shown in Figure 2.[13,15] HO_2 absorbs very weakly at 260 nm and therefore does not interfere significantly with CH_3O_2 detection.

Absorbance measurements at wavelengths below 220 nm were considered unsuitable because the quality of the signal falls off sharply due to both the response of the photomultiplier tube (PMT) and the Xe lamp output. Typically, 400 individual decays from the PMT are coadded and averaged to produce a

TABLE 1: Reactions Used To Model Peroxy Radical Kinetics at 150 Torr < *P* < 250 Torr

no. in text	reaction	k (cm^3 $molecule^{-1}s^{-1}$)	ref
13	$CH_3OH + Cl \rightarrow CH_2OH + HCl$	5.50×10^{-11}	11
14	$O_2 + CH_2OH \rightarrow HO_2 + CH_2O$	9.60×10^{-12}	11
9	$HO_2 + HO_2 \rightarrow HOOH + O_2$	$2.8 \times 10^{-13}\ e^{(594/T)}$	15
16	$CH_4 + Cl \rightarrow CH_3 + HCl$	$6.6 \times 10^{-12}\ e^{(-1240/T)}$	11
17	$CH_3 + O_2 + M \rightarrow CH_3O_2 + M$	$k_0 = (4.49 \times 10^{-31}) \times [M](T/298)^{-3.0}$ $k_\infty = 1.79 \times 10^{-12}\ (T/298)^{-1.7}$ $F_c = 0.6$	12
11a	$CH_3O_2 + CH_3O_2 \rightarrow 2CH_3O + O_2$	$1.0 \times 10^{-13}\ e^{(365/T)}$	11
11b	$\rightarrow CH_3OH + CH_2O + O_2$	$k_{11a}/k_{11b} = 0.4$[a]	
12	$HO_2 + CH_3O_2 \rightarrow CH_3OOH + O_2$	$3.8 \times 10^{-13}\ e^{(800/T)}$	12
18	$CH_3 + Cl_2 \rightarrow CH_3Cl + Cl$	$4.78 \times 10^{-12}\ e^{(-240/T)}$	23
19	$CH_3 + Cl \rightarrow CH_3Cl$	2.56×10^{-10}	24
20a	$Cl + CH_3O_2 \rightarrow CH_3O + ClO$	7.3×10^{-11}	15
20b	$\rightarrow CH_2OO + HCl$	7.6×10^{-11}	
21	$ClO + CH_3O_2 \rightarrow CH_3O + ClOO$	$4.9 \times 10^{-12}\ e^{(-330/T)}$	22
22	$CH_3O + O_2 \rightarrow CH_2O + HO_2$	$7.2 \times 10^{-14}\ e^{(-1080/T)}$	11
23	$CH_3O + CH_3O \rightarrow CH_2O + CH_3OH$	3.85×10^{-11}	25
24	$CH_3O_2 + CH_3O \rightarrow$ products	2.62×10^{-12}	26

[a] k_{11a}/k_{11b} product branching ratio taken from ref 27.

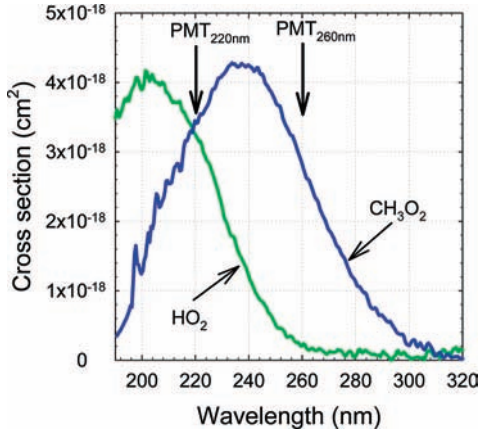

Figure 2. Comparison of UV cross sections for HO_2 and CH_3O_2. Arrows indicate the wavelengths used to measure the HO_2 and CH_3O_2 radical concentrations.

decay signal with good signal-to-noise. The oscilloscope (Tektronix model 460A, sampling rate 2 μs/pt and 12 bit resolution) is triggered by a photodetector activated by the photolysis laser flash. Transient behavior is recorded for 0.5 ms before photolysis and 4.5 ms after photolysis using a data acquisition rate of 2 μs/pt. This provides the appropriate time resolution and span to monitor the transient behavior of the peroxy radical chemistry.

B. Water Concentration Measurements. ***Bubbler.*** Water vapor is introduced into the reaction cell by N_2 carrier gas passing through a bubbler immersed in a constant temperature bath. The amount of water is controlled by both the temperature of the water and the flow rate of the carrier gas. The water vapor concentration was varied between 2 and 30 $\times$ 10^{16} molecules cm^{-3}. At the lower temperatures efforts were made to introduce water vapor as close as possible to the saturation vapor pressure, but the resultant uncertainties in exact water concentrations likely contribute to some of the increased scatter in these data.

IR Detection of Water Vapor. Tunable diode laser (TDL) IR spectroscopy is used to quantify the water in the cell. Figure 1 shows the IR system components, illustrating the use of separate lock-in amplifiers and detectors for the reaction cell and the reference cell. The water absorbs IR light that is scanned over a narrow frequency band centered at the 1524 cm^{-1} line such that the entire peak of the selected rovibration transition can be observed. The IR beam is produced by a Pb-salt TDL (Laser Components) that is tuned by a current and temperature controller (Laser Photonics model L5830) and mounted in an LN_2 dewar (Laser Photonics model L5736). The beam passes through a monochromator that determines its IR frequency, ± 1 cm^{-1}, and a 400 Hz chopper. It then passes through a beam splitter where a portion of the beam is directed through a reference cell containing a sample of water vapor ($\sim$2 Torr, 10 cm length). The remainder of the beam is directed to the reaction cell. After the signal propagates through the reaction cell, a second monochromator (Instruments SA, Inc. model HR 640, 75 line/mm, 10 μm blaze grating) filters the beam, which is then directed to an LN_2 cooled, AC coupled, HgCdTe detector. The modulated signal from the IR detector is converted to a low noise, highly stable, DC output by a lock-in amplifier (Stanford Research Systems model SR850) that receives a reference signal from the chopper. A function generator (Wavetek model 29) externally ramps the output of the diode laser with a frequency of 0.1 Hz with 500 mV (peak to peak). This results in the IR frequency of the diode laser scanning across the water line of interest, covering a range of 0.2 cm^{-1}. The beam passing through the reference cell is focused onto a second HgCdTe detector, and its signal is sent to a second lock-in amplifier (Spectra-Physics Model SP5020). The output signals for both detectors are recorded synchronously by a digital oscilloscope (Tektronix model 460A).

Determination of the Cross Section of Water. A syringe pump delivery system was used to introduce a known amount of water into the reaction cell over total pressures ranging from 50 to 700 Torr. Similar to quantifying methanol, the vapor concentration of water is calculated from the molar concentration using the syringe delivery rate, and the density and molecular weight of water. The flow rate of the carrier gas in standard liters per minute and the temperature and pressure of the mixture in the cell are needed to determine the $[H_2O]$ for the range of conditions covered in this study. The water vapor concentration is adjusted by changing the syringe delivery rate and/or the carrier gas flow rate. The syringe pump cannot deliver sufficient water vapor at the reactant flow rates used in the kinetics measurements, so it was replaced by the bubbler. The water vapor concentration is monitored via the same method described here.

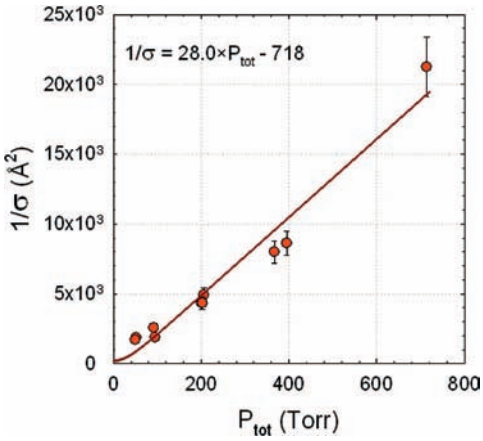

Figure 3. Pressure dependent cross section of water vapor at 1524 cm^{-1} measured at 295 K. [H_2O] is controlled by a syringe pump. Error bars show 10% error in the measured values. Line indicates peak intensity based on pressure and Doppler broadening.

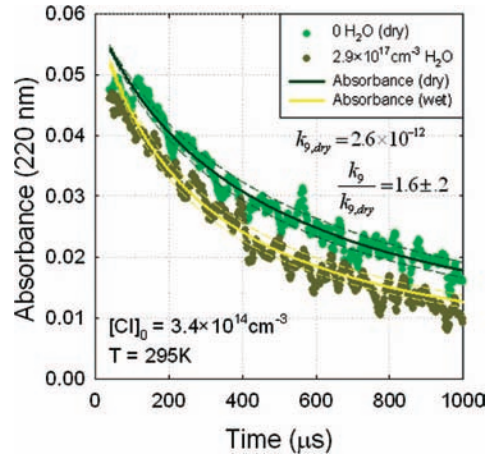

Figure 4. HO_2 self-reaction decays. Conditions: 175 Torr, 295 K, 0.7 Torr of CH_3OH, 0.30 Torr of Cl_2, 21 Torr of O_2. Dashed lines show 10% uncertainty in the rate constant.

The water absorbance is calculated via Beer's law from the ratio of IR intensities through a dry cell (I_0) versus a wet cell (I), where the bath gas is nitrogen:

$$\ln\left(\frac{I_0}{I}\right) = \sigma l c \qquad (15)$$

Here σ is the cross section of the absorbing species, l is the path length, and c is the concentration of the absorber. In this way the peak cross section of the 1524 cm^{-1} line is determined to be $2.0 \pm 0.2 \times 10^{-20}$ cm^2 at 200 Torr of N_2 and 295 K. The pressure dependence over the 50 to 700 Torr range is depicted in Figure 3. Rovibrational lines exhibit both Doppler and pressure broadening, with the latter dominating above ~10 Torr. In this regime, the line width increases linearly with collision frequency as modeled by a Lorentzian line shape; thus, the peak intensity exhibits the inverse dependence illustrated by Figure 3. Below ~10 Torr the line width reaches a Doppler limited minimum that is pressure independent. Owing to the $T^{1/2}$ dependence of collision frequency, pressure broadening only varies by ±3% over the 263−303 K range. In comparison, operation of the syringe pump and temperature control of the bubbler introduce roughly 10% uncertainty into the water vapor concentration.

III. Results

The instrument and data collection technique are verified by investigating the HO_2 self-reaction rate as a function of water vapor and temperature. This reaction is an ideal candidate for calibration because the water vapor and temperature dependence have been previously reported.[2−5] Figure 4 shows typical HO_2 radical absorbance/time decays which clearly demonstrate the self-reaction rate enhancement in the presence of water vapor.

The time/voltage traces collected by the PMT can be converted to time/concentration traces using eq 15, where I_0 is the averaged pretrigger signal of each trace. But for consistency with the analysis of CH_3O_2 kinetics below, the traces are left in terms of absorbance. The reaction model is run to produce a predicted [HO_2] concentration decay (using Micromath Scientist version 2.01 to solve the coupled differential equations that describe the kinetics), that is then converted to an absorbance at 220 nm (a small, <~8%, contribution is included for the absorbance at 220 nm by H_2O_2). The best fit of this model calculation to the data yields a self-reaction rate constant of $k_{9,dry} = (2.7 \pm 0.5) \times 10^{-12}$ cm^3 $molecule^{-1}$ s^{-1} at 295 K and with no water vapor present.

In contrast, at 295 K and 2.9×10^{17} molecules H_2O cm^{-3}, the rate of HO_2 decay increases, leading to an apparent rate constant of $k_9 = k_{9,dry}(1 + k_{9,w}[H_2O]) = (4.3 \pm 0.4) \times 10^{-12}$ cm^3 $molecule^{-1}$ s^{-1} that is enhanced by a factor of $k_9/k_{9,dry} = 1.6 \pm 0.2$ relative to the dry value. The error in $k_{9,dry}$ and $k_{9,w}$ is composed of the uncertainty in the fit to the data (95% confidence) and also includes contributions from the sources listed in the error section. The overall uncertainty is calculated by treating the various error sources as statistically independent. As systematic uncertainties in the reaction model cancel, the error in the enhancement includes only the reproducibility in the paired (with and without water) HO_2 absorbance decay rates.

The water enhancement increases with decreasing temperature. In this work we find an enhancement of 1.8 ± 0.1 at 283 K and 2.7×10^{17} molecules H_2O cm^{-3}. This compares favorably with the work of Kircher and Sander, who found the same factor of ~1.8 at 285 K, 100 Torr, and with a similar water vapor concentration.[5] The HO_2 self-reaction rate coefficient was measured under three different water vapor concentrations at four temperatures ranging between 273 and 303 K. Typically, a measurement was first conducted without the introduction of water vapor into the reaction cell (dry conditions), followed by a measurement with water vapor added (wet conditions). This was done in order to minimize changes in the gas flows and consequently changes in the gas mixtures. Figure 5 plots the HO_2 self-reaction enhancement factors recorded in this study as a function of water vapor concentration and temperature.

Maricq and Szente[16] reported the dry self-reaction rate as $k_{9,dry} = (2.8 \pm 0.5) \times 10^{-13}$ $e^{(594\pm55)/T}$ cm^3 $molecule^{-1}$ s^{-1}. The present dry measurements yield slightly higher rate constants, but this is due to an enhancement by methanol (used as the HO_2 precursor) as reported by Christensen et al.[17] After correction for the methanol enhancement, and fixing the activation energy (E_a/R) at −594 K because of the limited temperature range of the present data, fits of the dry HO_2 self-reaction rate constant to an Arrhenius expression yield $k_{9,dry} = (3.3 \pm 0.5) \times 10^{-13}$ $e^{(594/T)}$ cm^3 $molecule^{-1}$ s^{-1}, which is in reasonable agreement with the earlier result.

The water vapor dependence of the HO_2 self-reaction can be incorporated into the overall reaction rate coefficient via the [H_2O] dependent multiplicative factor introduced via equation 10. Keeping the $E_a/R = -594$ K value for the dry component and adopting the literature value of $E_a/R = -2200$ K for the

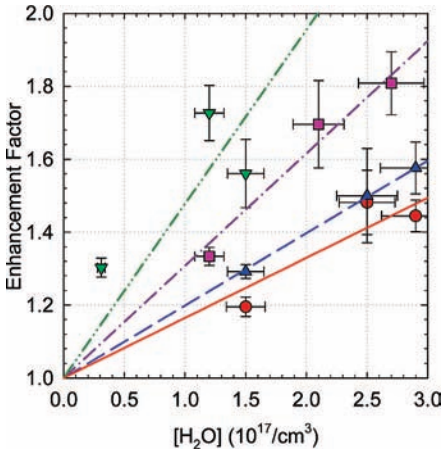

Figure 5. Enhancement ($k_9/k_{9,dry}$) for HO_2 self-reaction rates performed at ~200 Torr. Temperatures are indicated as follows: red circles, 303 K; blue triangles, 295 K; purple squares, 283 K; green upside-down triangles, 273 K.

wet component, the rate constants measured in the present work can be summarized by an HO_2 self-reaction rate constant of $k_9 = (3.4 \pm 0.5) \times 10^{-13}\ e^{(594/T)}\ (1 + (2.4 \pm 1.2) \times 10^{-21}\ e^{(2200/T)}\ [H_2O])$ cm^3 molecule^{-1} s^{-1} where the uncertainties are reported as the error in the fit to the data as well as the contributions from the sources listed in the error section. This result compares favorably with the work of Kircher and Sander,[5] who report a value of $2.3 \times 10^{-13}\ e^{(600/T)}\ (1 + 1.4 \times 10^{-21}\ e^{(2200/T)}\ [H_2O])$ cm^3 molecule^{-1} s^{-1}.

CH_3O_2 + CH_3O_2. If the kinetics of the CH_3O_2 self-reaction were to show a water vapor dependence, it would likely be due to the formation of a $CH_3O_2 \cdot H_2O$ complex, analogous to the HO_2 self-reaction. Information about the probability of $CH_3O_2 \cdot H_2O$ complex formation, including its binding energy, minimum energy structure and equilibrium constant, was reported in the study by Clark et al.[10] Due to the relatively weak binding energy of the $CH_3O_2 \cdot H_2O$ complex (2.3 kcal mol^{-1}) and consequently small equilibrium constant (1.54×10^{-21} cm^3 molecule^{-1}), it is unlikely that a sufficient concentration of the complex exists under atmospheric conditions. At the H_2O concentrations used in this study, the predicted fraction of methylperoxy radicals complexed with water at 295 K ranges from 0.02 to 0.05%. This is substantially lower than the fraction of 7.8−15% for the $HO_2 \cdot H_2O$ complex under the same conditions (based on the Kanno[9] equilibrium constant of $K_{eq} = (5.2 \pm 3.2) \times 10^{-19}$ cm^3 molecule^{-1} at 293 K).

The CH_3O_2 self-reaction rate coefficient in the presence of water vapor was measured using the same instrument/technique described above. Figure 6 shows the time decays of the CH_3O_2 absorbance in the absence and presence of water vapor at 295 K. These clearly demonstrate the lack of a water dependence on the CH_3O_2 self-reaction rate coefficient, consistent with theoretical expectations.

The chemistry of CH_3O_2 is more complex than for HO_2. The principal reactions used to model the decay of CH_3O_2 include the following.

Primary reactions:

$$Cl + CH_4 \rightarrow CH_3 + HCl \quad (16)$$

$$CH_3 + O_2 + M \rightarrow CH_3O_2 + M \quad (17)$$

$$CH_3O_2 + CH_3O_2 \rightarrow CH_3O + CH_3O + O_2 \quad (11a)$$

$$\rightarrow CH_3OH + CH_2O + O_2 \quad (11b)$$

$$CH_3O_2 + CH_3O_2 \cdot H_2O \rightarrow \text{products} \quad (11')$$

Competing reactions:

$$Cl_2 + CH_3 \rightarrow CH_3Cl + Cl \quad (18)$$

$$Cl + CH_3 \rightarrow CH_3Cl \quad (19)$$

$$Cl + CH_3O_2 \rightarrow CH_3O + ClO \quad (20a)$$

$$\rightarrow CH_2OO + HCl \quad (20b)$$

$$ClO + CH_3O_2 \rightarrow CH_3O + ClOO \quad (21)$$

Secondary reactions:

$$CH_3O + O_2 \rightarrow CH_2O + HO_2 \quad (22)$$

$$CH_3O + CH_3O \rightarrow CH_2O + CH_3OH \quad (23)$$

$$HO_2 + HO_2 \rightarrow HOOH + O_2 \quad (9)$$

$$HO_2 + CH_3O_2 \rightarrow CH_3OOH + O_2 \quad (12)$$

$$CH_3O_2 + CH_3O \rightarrow \text{products} \quad (24)$$

At the ~200 Torr of the present experiments the O_2 addition to CH_3 is in the falloff region; hence the full pressure dependent rate constant for reaction 17 is employed in the model (Table 1). Reactions 18 and 19 remove CH_3, but have little effect on the kinetics due to the large abundance of O_2 in the reaction cell. The lifetime of CH_3 with respect to O_2 is calculated to be <1 μs under the conditions used in this study. The short lifetime effectively removes CH_3 before it can participate in the competing reactions 18 and 19. The production of HO_2 from reaction 22 leads to secondary removal of CH_3O_2 that is accounted for by the model.

The largest interference comes from ClO. Unlike the rapid formation of HO_2 from methanol, the formation of CH_3O_2 by the Cl + CH_4 route is slow enough to allow about 3−4% of the photolyzed Cl atoms to react with the peroxy radical and produce ClO (reaction 20a). This has two consequences: (1) interference with the CH_3O_2 decay chemistry, reaction 21, and (2) optical interference with the UV absorbance measurement at 260 nm. Adding the ClO chemistry to the model has a 20% effect on the best fit rate constant, mainly through the ClO reaction with CH_3O_2. A sensitivity analysis of the model to the ClO + CH_3O_2 reaction rate coefficient showed that changing this reaction rate coefficient by ±30% relative to the recom-

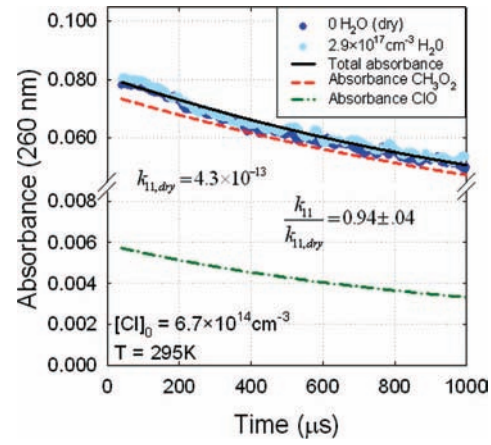

Figure 6. CH_3O_2 self-reaction decays. Conditions: 250 Torr, 295 K, 100 Torr of CH_4, 0.32 Torr of Cl_2, 21 Torr of O_2. Measured absorbances are indicated by the symbols. The lines represent predicted total absorbance as well as the contributions from CH_3O_2 and ClO, with water vapor present ("dry" data is essentially identical).

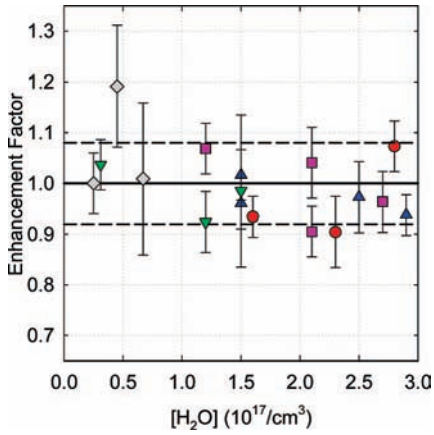

Figure 7. Enhancement ($k_{11}/k_{11,dry}$) for CH_3O_2 self-reaction rates performed at ~200 Torr. Temperatures are indicated as follows: red circles, 303 K; blue triangles, 295 K; purple squares, 283 K; green upside-down triangles, 273 K; gray diamonds, 263 K.

mended value found in the JPL evaluation[12] resulted in a <5% change in k_{11}.

Second, the UV spectrum of ClO near 260 nm is very similar to that of CH_3O_2, except 1.8 times as intense, hence the choice to fit the absorbance traces rather than attempting to convert them to CH_3O_2 concentrations. Thus, the model calculates predicted CH_3O_2 and ClO concentration decays, converts these to the corresponding 260 nm absorbances, and compares their sum to the measured decay curves. Figure 6 demonstrates the best fit to the data. Superimposed are the CH_3O_2 and ClO absorbances, with the latter contributing <10%. In principle, UV absorption at 260 nm by the secondary HO_2 radicals can contribute a similar interference. However, due to its small cross section at 260 nm, the HO_2 contribution to the overall absorbance remains under 0.3%.

At 295 K, the "dry" self-reaction rate constant is $k_{11,dry} = (3.9 \pm 0.9) \times 10^{-13}$ cm^3 molecule^{-1} s^{-1} (average of 4 measurements), whereas an average "wet" self-reaction rate constant of $k_{11,dry}(1 + k_{11,w}[H_2O]) = (3.8 \pm 0.8) \times 10^{-13}$ cm^3 molecule^{-1} s^{-1} is found, independent of water vapor concentration. Even with the maximum amount of water vapor, the observed decay appears not to be perturbed, as predicted by the K_{eq} calculated by Clark et al.[10] Three different water vapor concentrations were measured at five temperatures ranging between 263 and 303 K for the CH_3O_2 self-reaction.

Figure 7 shows the observed rate enhancement as a function of water vapor concentration for the various experimental temperatures. The solid line through the figure shows the average enhancement, which lies at unity. Table 2 lists absolute rate constants determined in this study over the temperature and water vapor ranges. Atkinson et al.[11] reported a temperature dependent self-reaction rate of $k_{11} = 1.0 \times 10^{-13}$ e$^{(365\pm201)/T}$ cm^3 molecule^{-1} s^{-1}. A fit of the present rate constants to the Arrhenius expression, fixing the activation energy at the literature value, yields a value of $k_{11} = (1.1 \pm 0.1) \times 10^{-13}$ e$^{365/T}$ cm^3 molecule^{-1} s^{-1}. The uncertainty is calculated from the fit to the data and also includes contributions from the sources listed in the error section.

$CH_3O_2 + HO_2$. Measurement of the $CH_3O_2 + HO_2$ reaction rate coefficient as a function of water vapor and temperature does not show any enhancement over the range examined. Only the CH_3O_2 concentration is monitored for these experiments because any enhancement in the HO_2 decay rate due to the $CH_3O_2 + HO_2$ reaction would be masked by the enhancement of its self-reaction. Also, the CH_3O_2 self-reaction is much slower

TABLE 2: Absolute Rate Constants for CH_3O_2 Self-Reaction with and without Water as a Function of Temperature and Water Vapor Concentration[a]

	303 K		295 K		283 K		273 K		263 K	
[H$_2$O] (10^{17} cm^{-3})	k_w	k_{dry}	k_w	k_{dry}	k_w	k_{dry}	k_w	k_{dry}	k_w	k_{dry}
2.8	3.8	3.6								
2.3	3.0	3.3								
1.6	3.5	3.8								
2.9			4.0	4.3						
2.5			4.7	4.8						
1.5			2.7	2.8						
1.5			3.7	3.6						
2.7					3.4	3.6				
2.1					4.9	4.7				
2.1					2.4	2.6				
1.2					3.6	3.4				
1.5							4.6	4.7		
1.2							4.5	4.9		
0.3							4.5	4.4		
0.7									4.6	4.5
0.5									4.2	3.6
0.3									3.6	3.6

[a] The total pressure is ~200 Torr. Experimental uncertainty is 10%. The units are 10^{-13} cm^3 s^{-1}.

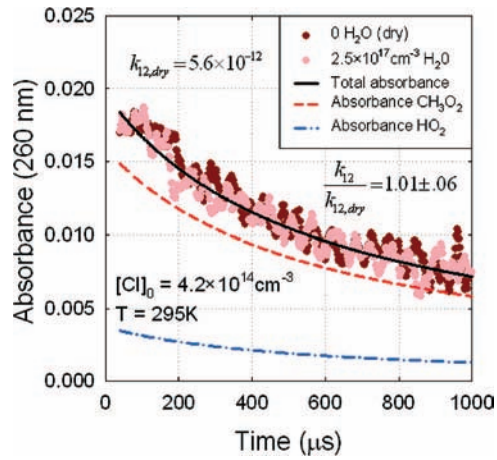

Figure 8. $CH_3O_2 + HO_2$ reaction decays. Conditions: 250 Torr, 295 K, 99 Torr of CH_4, 0.6 Torr of CH_3OH, 0.30 Torr of Cl_2, 21 Torr of O_2. Measured absorbances are indicated by the symbols. The lines represent predicted total absorbance as well as the contributions from CH_3O_2 and HO_2, with water vapor present ("dry" data is essentially identical).

than the $CH_3O_2 + HO_2$ reaction, so any change in the CH_3O_2 decay rate due to the cross-reaction would be more readily observed. The initial concentration ratio of CH_3O_2 to HO_2 was biased to favor HO_2 to ensure that there was sufficient HO_2 to sustain the cross-reaction. The initial radical ratio, $[HO_2]/[CH_3O_2]$, was varied between 2.5 and 4.7. There was no effect on the measured rate constant as a function of initial radical concentrations. Figure 8 shows the decay of CH_3O_2 absorbance, with and without water vapor, under conditions in which the initial concentrations of HO_2 and CH_3O_2 are approximately equal. At 295 K, $k_{12,dry} = (6.1 \pm 1.1) \times 10^{-12}$ cm^3 molecule^{-1} s^{-1} and $k_{12,dry}(1 + k_{12,w}[H_2O]) = (6.0 \pm 1.5) \times 10^{-12}$ cm^3 molecule^{-1} s^{-1}, which is the average of the values from Table 3. Fitting our temperature dependent data to an Arrhenius expression yields $k_{12} = (3.6 \pm 0.4) \times 10^{-13}$ e$^{800/T}$ cm^3 molecule^{-1} s^{-1}, where the activation energy of $E_a/R = -800$ K is fixed at the literature value.[11] The resulting A-factor of $(3.6 \pm 0.4) \times 10^{-13}$ cm^3 s^{-1} is in good agreement with the previously reported value of 3.8×10^{-13} cm^3 s^{-1}.[10]

TABLE 3: Absolute Rate Constants for the $CH_3O_2 + HO_2$ Reaction with and without Water Vapor as a Function of Temperature and Water Vapor Concentration[a]

	303 K		295 K		283 K		273 K		263 K	
$[H_2O]$ (10^{17} cm^{-3})	k_w	k_{dry}	k_w	k_{dry}	k_w	k_{dry}	k_w	k_{dry}	k_w	k_{dry}
2.8	7.8	7.2								
2.3	5.8	5.3								
1.6	6.2	5.8								
2.9			8.2	7.6						
2.5			5.6	5.6						
1.5			4.8	4.9						
1.5			5.5	6.1						
2.7					5.3	5.0				
2.1					6.8	6.6				
1.2					7.9	7.4				
1.5							4.3	5.1		
1.2							4.8	5.6		
0.3							4.6	4.8		
0.5									7.8	7.3
0.3									7.8	7.4

[a] The total pressure is ~200 Torr. Experimental uncertainty is 10%. The units are 10^{-12} cm^3 s^{-1}.

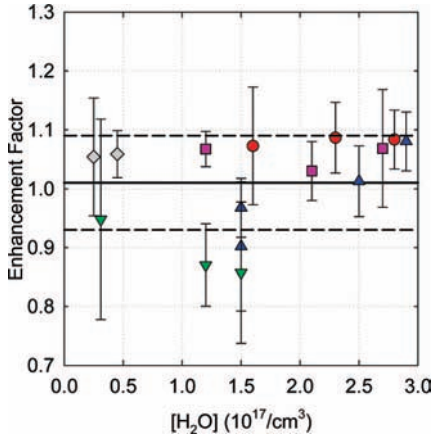

Figure 9. Enhancement ($k_{12}/k_{12,dry}$) for $CH_3O_2 + HO_2$ reaction rates performed at ~200 Torr. Temperatures are indicated as follows: red circles, 303 K; blue triangles, 295 K; purple squares, 283 K; green upside-down triangles, 273 K; gray diamonds, 263 K.

This cross-reaction is likewise more complex than the HO_2 self-reaction. However, the same reaction scheme used above for the CH_3O_2 self-reaction suffices to model the decay of CH_3O_2 when HO_2 is present. As a result of using CH_3OH to generate HO_2 radicals, the Cl atom concentration diminishes more quickly than it does in the CH_3O_2 self-reaction case. Therefore, ClO does not form in significant amounts, and the contribution to the measured absorbance is negligible.

Three different water vapor concentrations were measured at five temperatures ranging between 263 and 303 K for the $CH_3O_2 + HO_2$ reaction, with the exception of only 2 concentrations at 263 K. The enhancement factor is always calculated from reactions run in pairs and under the same conditions, varying only the presence or absence of water vapor. Figure 9 shows the observed enhancement as a function of water vapor concentration for the temperatures investigated. The solid line represents the average enhancement over all measurements, and the dashed lines provide error bounds. Table 3 lists the absolute rate constants determined in this study.

Error Analysis. ***Measurement Errors.*** Sources of uncertainty include the total pressure of the reaction cell from averaging the readings at the ends of the cell (±2%) and from the MKS pressure gauges which have an accuracy better than ±1%; K-type thermocouples measure the temperature at the ends of the cell and show a gradient of 2%; uncertainty in the partial pressures of the gases is due to the measured flow rates (±2%) and the pressure gauges. Typically, 400 averages of the transient trace from the PMT are accumulated to improve the signal-to-noise, but this also avoids issues related to laser energy variation (<5%) which contributes to uncertainty in the $[Cl]_0$. Chopper modulation is used to measure the signal amplitude (I_0) with an accuracy of ±1 mV (0.25%). The statistical composite of these instrumental uncertainties produces an approximately 5% contribution to the overall error bounds for the reported rate coefficients.

Kinetic Model Uncertainties. The kinetics model uses a Jacobian Matrix to calculate the uncertainty in the best fit rate constants. Uncertainty is reported at a 95% confidence level from the best fits to the individual absorbance decays. Referenced rate constant values are used in the model without any modifications. The small uncertainties in the precursor gas concentrations do not affect the predictions of the model. A sensitivity analysis of the model to the precursor gas concentrations shows that changing the $[CH_4]$ by ±10% affects the predicted k_{11} by less than 10%.

Besides the ClO interference discussed above, the model for the CH_3O_2 self-reaction is most sensitive to the $Cl + CH_4$ reaction rate coefficient. The uncertainty here is small at 295 K (5%), and changing k_{16} by this amount results in a <6% effect on k_{11}. The uncertainty in the $Cl + CH_4$ reaction rate coefficient grows with decreasing temperature. Propagating the uncertainty in this reaction rate coefficient at each experimental temperature results in an almost linear influence on the best fit of k_{11}. Consequently the overall contribution of model uncertainty to the error bound for k_{11} is 16%.

In the case of the cross-reaction, the major uncertainty comes from the value of $[CH_4]/[CH_3OH]$. Changing this ratio by ±10% in the model yielded up to a 15% variation in k_{12}. This is not unexpected, and it may explain the scatter in the absolute rate constants reported in Table 3. The overall contribution of model uncertainties to k_{12} is 15%.

The enhancement factors (k_{wet}/k_{dry}) are obtained from matched pairs (wet and dry) of photolysis measurements. Uncertainties arising from the model are therefore correlated and do not contribute to the enhancement error bounds. Instead, these are based on the scatter in experimental data, e.g., Figures 7 and 9.

IV. Conclusions

Water vapor when present can potentially complex with peroxy radicals and influence their chemistry. The enhancement of the self-reaction of HO_2 is very significant in the tropospheric production of hydrogen peroxide and may be due to two factors.[5] First, the water may be acting as an energy chaperone much like a third body except that the lifetime of the activated complex is no longer important since the third body is present already at its formation. Zhu and Lin[18] explain it as a catalytic reduction in the barrier of formation of the products. In the case of the $HO_2 \cdot H_2O$ complex, the "third body" is bound to the activated complex by 6.9 kcal mol^{-1}.[9] Second, the presence of water in the activated complex increases its number of degrees of freedom, thus increasing its lifetime and the chance of collisional stabilization.

Under the conditions examined in the present work, the CH_3O_2 self-reaction rate constant does not appear to be enhanced in the presence of water vapor. This is consistent with the low fraction of complexes that are present in equilibrium under atmospheric conditions, as expected from the small binding

energy.[10] The steady state concentration of $CH_3O_2 \cdot H_2O$ complexes is substantially lower than that of $HO_2 \cdot H_2O$ and, thus, enhancement of the methylperoxy self-reaction remains negligible. The results of this study are consistent with the water vapor effect reported in previous studies of Kurylo et al.[19,20] and Lightfoot et al.[21]

Kinetic studies on the cross-reaction between HO_2 and CH_3O_2 radicals indicate that the reaction rate constant is likewise not enhanced by water vapor under the conditions probed. This cannot be explained simply by a low steady state concentration of complex, since $HO_2 \cdot H_2O$ is involved in both the self- and cross-reactions. Perhaps in the case of the cross-reaction the higher number of vibrational modes already gives the intermediate complex a sufficiently long lifetime that the chaperone adds little to collisional stabilization. This could be investigated by studying the self-reactions of peroxy radicals with carbonyl or alcohol groups, which, from the work of Clark et al.,[10] have higher water binding energies. If they too lack a significant enhancement, it would indicate that the chaperone effect is not important for peroxy radicals larger than HO_2. Investigations using these types of systems are presently underway. It is hoped that the results from these studies will help clarify the mechanism responsible for the observed enhancement due to water vapor.

Acknowledgment. Recognition is made to the National Science Foundation (Grant No. 0631167) for support of the present work.

References and Notes

(1) Finlayson-Pitts, B. J.; Pitts, J. N. J. *Chemistry of the Upper and Lower Atmosphere: Theory, Experiments and Applications*; Academic Press: San Diego, 2000.
(2) Stone, D.; Rowley, D. M. *Phys. Chem. Chem. Phys.* **2005**, *7*, 2156.
(3) Kanno, N.; Tonokura, K.; Tezaki, A.; Koshi, M. *J. Phys. Chem. A* **2005**, *109*, 3153.
(4) Sander, S. P.; Peterson, M.; Watson, R. T.; Patrick, R. *J. Phys. Chem.* **1982**, *86*, 1236.
(5) Kircher, C. C.; Sander, S. P. *J. Phys. Chem.* **1984**, *88*, 2082.
(6) Stockwell, W. R. *J. Geophys. Res., [Atmos.]* **1995**, *100*, 11695.
(7) Suma, K.; Sumiyoshi, Y.; Endo, Y. *Science* **2006**, *311*, 1278.
(8) Aloisio, S.; Francisco, J. S. *J. Phys. Chem. A* **1998**, *102*, 1899.
(9) Kanno, N.; Tonokura, K.; Koshi, M. *J. Geophys. Res., [Atmos.]* **2006**, *111*, 020312.
(10) Clark, J.; English, A. M.; Hansen, J. C.; Francisco, J. S. *J. Phys. Chem. A* **2008**, *112*, 1587.
(11) Atkinson, R.; Baulch, D. L.; Cox, R. A.; Crowley, J. N.; Hampson, R. F.; Hynes, R. G.; Jenkin, M. E.; Rossi, M. J.; Troe, J. *Atmos. Chem. Phys.* **2006**, *6*, 3625.
(12) Sander, S. P.; Friedl, R. R.; Golden, D. M.; Kurylo, M. J.; Moortgat, G. K.; Wine, P. H.; Ravishankara, A. R.; Kolb, C. E.; Molina, M. J.; Finlayson-Pitts, B. J.; Huie, R. E.; Orkin, V. L. *Chemical Kinetics and Photochemical Data for Use in Atmospheric Studies Evaluation Number 15*; Jet Propulsion Laboratory: Pasadena, CA, 2006.
(13) Maricq, M. M.; Wallington, T. J. *J. Phys. Chem.* **1992**, *96*, 986.
(14) Bryukov, M. G.; Dellinger, B.; Knyazev, V. D. *J. Phys. Chem. A* **2006**, *110*, 936.
(15) Maricq, M. M.; Szente, J. J. *J. Phys. Chem.* **1994**, *98*, 2078.
(16) Maricq, M. M.; Szente, J. J.; Kaiser, E. W.; Shi, J. C. *J. Phys. Chem.* **1994**, *98*, 2083.
(17) Christensen, L. E.; Okumura, M.; Hansen, J. C.; Sander, S. P. *J. Phys. Chem. A* **2006**, *110*, 6948.
(18) Zhu, R. S.; Lin, M. C. *Chem. Phys. Lett.* **2002**, *354*, 217.
(19) Dagaut, P.; Wallington, T. J.; Kurylo, M. J. *J. Phys. Chem.* **1988**, *92*, 3833.
(20) Kurylo, M. J.; Dagaut, P.; Wallington, T. J.; Neuman, D. M. *Chem. Phys. Lett.* **1987**, *139*, 513.
(21) Lightfoot, P. D.; Veyret, B.; Lesclaux, R. *J. Phys. Chem.* **1990**, *94*, 708.
(22) Atkinson, R.; Baulch, D. L.; Cox, R. A.; Hampson, R. F.; Kerr, J. A.; Rossi, M. J.; Troe, J. *J. Phys. Chem. Ref. Data* **1997**, *26*, 521.
(23) Timonen, R. S.; Seetula, J. A.; Gutman, D. *J. Phys. Chem.* **1990**, *94*, 3005.
(24) Timonen, R.; Kalliorinne, K.; Koskikallio, J. *Acta Chem. Scand., Ser. A* **1986**, *40*, 459.
(25) Hassinen, E.; Koskikallio, J. *Acta Chem. Scand., Ser. A* **1979**, *33*, 625.
(26) Heicklen, J. *Adv. Photochem.* **1988**, *14*, 177.
(27) Tyndall, G. S.; Wallington, T. J.; Ball, J. C. *J. Phys. Chem. A* **1998**, *102*, 2547.

JP800727A